

Fe I oscillator strengths for transitions from high-lying odd-parity levels

M. T. Belmonte, J. C. Pickering, M. P. Ruffoni

Blackett Laboratory, Physics Department, Imperial College London, London SW7 2AZ, UK

`m.belmonte-sainz-ezquerra@imperial.ac.uk`

E .A. Den Hartog, J. E. Lawler and A. Guzman

Department of Physics, University of Wisconsin-Madison, Madison, WI 53706.

U. Heiter

Observational Astrophysics, Department of Physics and Astronomy, Uppsala University,

Box 516, 751 20 Uppsala, Sweden

Received _____; accepted _____

ABSTRACT

We report new experimental Fe I oscillator strengths obtained by combining measurements of branching fractions measured with a Fourier Transform spectrometer and time-resolved laser-induced fluorescence lifetimes. The study covers the spectral region ranging from 213 to 1033 nm. A total of 120 experimental $\log(gf)$ -values coming from 15 odd-parity energy levels are provided, 22 of which have not been reported previously and 63 values with lower uncertainty than the existing data. Radiative lifetimes for 60 upper energy levels are presented, 39 of which have no previous measurements.

Subject headings: atomic data — line: profiles — methods: laboratory — techniques: spectroscopic

1. Introduction

Iron is one of the most studied elements within the field of astronomy due to its important presence in stellar spectra. With a very complex spectrum, neutral iron presents thousands of transitions across a very wide spectral range, from the ultraviolet to the infrared. A very comprehensive study of its spectrum was undertaken by Nave et al. (1994), which provides an extremely useful guide for the identification of Fe I spectral lines in astronomical spectra. However, of the 6758 lines included in the National Institute of Standards and Technology (NIST) atomic database in the spectral interval ranging from 200 to 1050 nm, only a small percentage possess accurate values of transition probabilities.

Atomic oscillator strengths (transition probabilities, $\log(gf)$) are essential to model stellar line intensities and calculate not only chemical abundances, but also other stellar parameters. In particular, the iron spectrum is of the utmost importance to obtain stellar metallicities, as this property is directly linked to the iron abundance. However, the quantity and quality of the existing data lies far from the current needs of the astronomical community, remaining the Achilles' heel of the field of Galactic archaeology (Bigot and Thévenin 2006). Several attempts have been made to assemble comprehensive line lists with reliable atomic data (Heiter et al. 2015b) which can be used as a standard input for the different LTE and non-LTE models used to determine chemical abundances.

Several studies regarding the measurement of oscillator strengths of neutral iron have been conducted over the last fifty years. A very detailed review of the situation was carried out ten years ago by Fuhr and Wiese (2006), where they present the most comprehensive compilation of Fe I transition probabilities to date which states clearly the need for new studies that complete and improve the quality of thousands of spectral lines in the database of Fe I $\log(gf)$ values. Amongst all the works whose values are included in Fuhr and Wiese (2006), two deserve special attention due to the quality of their results and their coverage.

These are the experiments conducted by Blackwell et al. (1979a, 1979b, 1980, 1982a, 1982b and 1986) and O’Brian et al. (1991).

Very accurate absorption oscillator strengths were obtained by Blackwell et al. from a very stable light source in an absorption experiment, with estimated uncertainties lower than $\pm 4\%$ on an absolute scale. Their values are generally considered as the most reliable ones by Fuhr and Wiese (2006), who rated them as ‘A’ in their compilation. The comprehensive work from O’Brian et al. (1991) provides accurate transition probabilities for 1814 spectral lines of neutral iron obtained in an emission experiment by using two different methods. One method combines radiative lifetimes of 186 energy levels with measurements of branching fractions yielding 1174 absolute transition probabilities. The other method used by O’Brian et al interpolated the populations of energy levels using those with known lifetimes in an inductively coupled plasma source, producing 640 extra transition probabilities with uncertainties that they estimated to be lower than $\pm 10\%$. Within the spectral range included in our new study, the majority of the $\log(gf)$ -values available for comparison belong to O’Brian et al. (1991).

Our new work is the third in a series of articles published as a result of the collaboration between the Fourier Transform Spectroscopy laboratory at Imperial College London (IC) and the University of Wisconsin-Madison (UW). It completes the previous works on $\log(gf)$ for Fe I lines of interest in the Gaia-ESO survey (Ruffoni et al. 2014) and oscillator strengths for transitions coming from high-lying even-parity Fe I levels (Den Hartog et al. 2014). In this paper we focus on the $\log(gf)$ values for transitions coming from high-lying odd-parity upper energy levels, four of which contain spectral lines of particular interest for the Gaia-ESO survey. We provide new radiative lifetimes for 60 high-lying odd-parity levels obtained at the UW, 39 of which are measured for the first time. Fe I emission spectra were recorded with the Fourier transform spectrometers at IC and at the National Institute of

Standards and Technology (NIST). Measurements of branching fractions were completed for 15 of the previously mentioned odd-parity levels, and were combined with the new lifetimes to obtain 120 accurate values of oscillator strengths (and transition probabilities). Comparison with previous experiments shows that 22 of the analysed transitions have no earlier $\log(gf)$ -values and for 63 transitions the accuracy of the $\log(gf)$ s are improved compared with existing measurements in the literature.

2. Experimental procedure

Oscillator strengths, or absorption f-values, are obtained experimentally from the measurement of atomic transition probabilities, A_{ul} , where the subscript ul refers to the transition from a given upper energy level, u , to a lower level, l . Transition probabilities and absorption f-values are related by (Thorne et al. 2007):

$$\log(g_l f) = \log \left[A_{ul} g_u \lambda^2 \times 1.499 \times 10^{-14} \right] \quad (1)$$

where g_l and g_u are the statistical weights of the lower and upper energy level, respectively, and λ is the wavelength of the line expressed in nm.

The transition probability of a given atomic transition can be obtained spectroscopically, since in the case of an optically thin plasma it is proportional to the area under the profile of the corresponding spectral line. The integrated area of each intensity calibrated spectral line, I_{ul} , is proportional to its intensity in photons per second (Pickering et al. 2001a).

So called Branching Fractions (Huber and Sandeman 1986) are given by:

$$BF_{ul} = \frac{I_{ul}}{\sum_l I_{ul}} = \frac{A_{ul}}{\sum_l A_{ul}} \quad (2)$$

and for a particular upper energy level the lifetime τ_u is:

$$\tau_u = \frac{1}{\sum_l A_{ul}}. \quad (3)$$

As long as the sum of the A_{ul} includes all branches to the lower energy levels, we can combine expressions 2 and 3 to obtain the transition probability of a given transition as:

$$A_{ul} = \frac{BF_{ul}}{\tau_u} \quad (4)$$

As can be seen, this method of measuring A_{ul} has the advantage that no assumption needs to be made regarding the thermodynamic equilibrium of the plasma used as a light source.

2.1. Branching fraction measurements

Two different sets of spectra were used to obtain the $\log(gf)$ values included in this work. Spectrum A was measured on the 2 m FT spectrometer at the National Institute of Standards and Technology (NIST) and it covers the spectral range between 8000 and 26000 cm^{-1} . An iron cathode mounted in a water cooled hollow cathode lamp (HCL) was used to generate the plasma used as light source. The HCL was run in Ne at a pressure of 2.1 mbar and a current 2 A. A detailed description of this measurement can be found in Ruffoni et al. (2014) and Den Hartog et al. (2014). The response function of the spectrometer, shown in Fig.1 for Spectrum A, was obtained by using a calibrated Standard tungsten (W) halogen lamp in the spectral range between 250 and 2400 nm. In order to verify that this spectrometer response was stable over time, spectra of this tungsten lamp (whose radiance is known to $\pm 1.1\%$) were measured before and after acquiring iron spectra with the HCL.

Spectra B, C, D and G were measured on the IC VUV Fourier Transform Spectrometer

(FTS) covering the spectral range between 20000 and 62000 cm^{-1} . The resolution, detector and filter used to record each spectrum, as well as the experimental conditions are included in Table 1. The Fe I emission spectra were produced in a water cooled HCL filled with Ne at a pressure ranging from 1.3 to 1.4 mbar and with a 99.8% pure iron cathode operated as the source. Currents of 700 or 1000 mA (see Table 1) were selected depending on the signal-to-noise ratio of the spectral lines of interest. These conditions were optimized to obtain the highest signal-to-noise ratio for the weaker lines, whilst avoiding self-absorption effects for the stronger lines.

Two Standard intensity calibrated lamps were used to obtain the response function of the IC VUV spectrometer for these four spectra: a deuterium lamp (D_2) in the spectral interval ranging from 200 to 350 nm and a tungsten lamp (W) for longwards of 300 nm. Spectra from these two lamps were measured before and after each of the runs recorded with the HCL lamp and using the same measurement conditions. The uncertainties of the relative spectral radiance of the W lamp, calibrated by the UK National Physical Laboratory (NPL) were lower than $\pm 1.4\%$ between 410 and 800 nm, increasing to $\pm 2.8\%$ at 300 nm. The deuterium lamp, calibrated by the Physikalisch-Technische Bundesanstalt (PTB) in Germany, has a relative spectral radiance with an uncertainty of $\pm 7\%$ between 170 and 410 nm. The response functions of the different spectra, shown in Fig.1, were obtained by combining the response functions found using both lamps, W and D_2 .

The Fe spectra were fitted by using Voigt profiles with the XGREMLIN package (Nave et al. 1997). Once fitted and intensity calibrated, the spectra were used to obtain the branching fractions of all the transitions coming from the upper energy levels of interest by using the FAST software package (Ruffoni et al. 2013a). The calculated branching fractions of Kurucz (2007) were used to define the transitions to be included, and to estimate the completeness of the set of transitions from each upper level considered, as described in

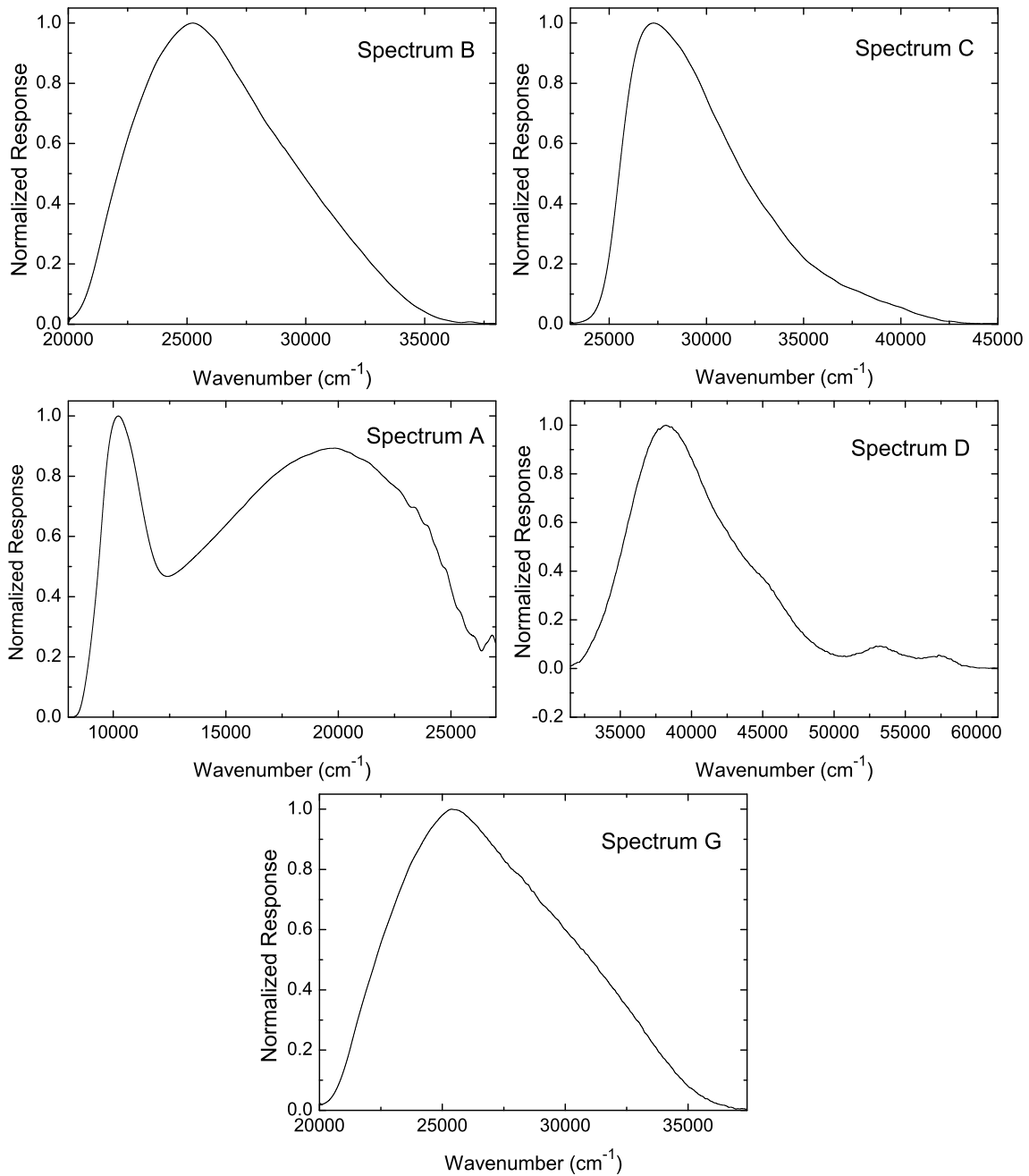


Fig. 1.— Response functions used to intensity calibrate the five different spectra used in this work (see Table 1).

Pickering et al. (2001a) and Pickering et al. (2001b). Final results for new $\log(gf)$ s were also obtained using the FAST software to combine the branching fractions with the new experimental upper energy lifetime values described in Section 2.2.

All the fitted spectral lines were checked for possible self-absorption by carefully examining the residuals from the line fits. Possible cases of blended lines were also analysed by checking the Fe I linelist of Nave et al. (1994) and Fe II linelist of Nave & Johansson (2013), as well as the theoretical $\log(gf)$ s of Kurucz (2007).

For most of the cases, more than one spectrum from Table 1 was necessary to encompass all the transitions coming from a given upper energy level. In these situations, all the lines were put on a common relative intensity scale by calculating the ratio in the intensity of several lines from that particular upper energy level which were measured in the overlapping region of the pairs of spectra. A detailed description of this method can be found in Pickering et al. (2001a) and Pickering et al. (2001b).

We have paid special attention to the calculation of the experimental uncertainties introduced in our BF measurements by taking into account all the different sources of error, such as the uncertainty in the signal-to-noise ratio of the observed Fe I spectral line and the standard calibration lamp spectra, as well as the spectral radiance uncertainty of these standard light sources. A detailed description can be found in Ruffoni et al. (2013a) and Ruffoni (2013b), but the general expression is included here for completeness. The experimental uncertainty of a given BF can be defined as:

$$\left(\frac{\Delta\text{BF}_{ul}}{\text{BF}_{ul}}\right)^2 = (1 - 2\text{BF}_{ul})\left(\frac{\Delta I_{ul}}{I_{ul}}\right)^2 + \sum_{j=1}^n \text{BF}_{uj}^2 \left(\frac{\Delta I_{uj}}{I_{uj}}\right)^2 \quad (5)$$

where I_{ul} is the calibrated relative intensity of the emission line associated with the electronic transition from level u to level l , and ΔI_{ul} is the uncertainty in intensity of this

line due to its measured signal-to-noise ratio and the uncertainty in the intensity of the standard lamp. From Equation 4, it then follows that the uncertainty in A_{ul} is:

$$\left(\frac{\Delta A_{ul}}{A_{ul}}\right)^2 = \left(\frac{\Delta \text{BF}_{ul}}{\text{BF}_{ul}}\right)^2 + \left(\frac{\Delta \tau_{ul}}{\tau_{ul}}\right)^2 \quad (6)$$

where $\Delta \tau_{ul}$ is the uncertainty in our measured upper level lifetime. Finally, the uncertainty in $\log(gf)$ of a given line can be calculated as:

$$\Delta \log(gf) = \log\left(1 + \frac{\Delta A_{ul}}{A_{ul}}\right) \quad (7)$$

2.2. Radiative lifetime measurements

Radiative lifetimes provide the absolute scale for the branching fractions. They are measured using time-resolved laser-induced fluorescence (TRLIF) on a slow beam of iron atoms. This beam is produced from a hollow cathode discharge sputter source. A pulsed electrical discharge is operated in ~ 50 Pa argon gas at 30 Hz repetition rate. The pulses have ~ 10 A peak current and 10 μs duration during which the energetic argon ions sputter atoms from the pure iron foil lining the stainless steel hollow cathode. The discharge is maintained between pulses with a 30 mA DC current. The cathode is closed on the downstream end except for a 1 mm flared hole, through which the gas phase iron is differentially pumped into the low pressure ($\sim 10^{-2}$ Pa) scattering chamber. The beam is weakly-collimated and slow (the neutrals have speeds of $\sim 5 \times 10^4$ cm.s^{-1} and the ions are somewhat faster), and contains both neutral and singly-ionized iron in their ground and low metastable levels.

The atomic/ionic beam is intersected at 90° angles by a beam from a nitrogen laser-pumped dye laser. This intersection takes place 1 cm below the bottom of the cathode.

The laser pulse is delayed relative to the peak of the discharge pulse by $\sim 20 \mu\text{s}$ to account for the transit time of the atoms. The duration of the laser is $\sim 3 \text{ ns}$ (FWHM) and the pulse terminates completely within a few nanoseconds. This latter characteristic allows the fluorescence to be recorded free from laser interaction, making it unnecessary to deconvolute the laser pulse and fluorescence signals. The wavelength of the laser is tunable over the range 205 - 720 nm using a large selection of dyes as well as frequency doubling crystals. The narrow bandwidth of the laser (0.2 cm^{-1}) ensures selective excitation of the level of interest. Cascade radiation from higher-lying levels, which troubled earlier, non-selective techniques such as beam foil excitation, is not a problem in this experiment.

A transition is chosen for laser excitation which is classified to the level of interest and has some observed intensity in the NIST line list for Fe I (Kramida et al. 2011)¹. The transition must also originate in the ground or low-lying metastable levels which are populated in the atomic beam. We find that neutral iron metastable levels up to $25\,000 \text{ cm}^{-1}$ have sufficient population for use as lower levels for laser excitation. Care must be taken to correctly identify the transition in the experiment, particularly when working in such dense spectra as Fe I, II. We do not rely on an absolute measurement of the laser wavelength. Rather, the wavelength is course-tuned to within 0.1 nm of the transition by adjusting the grating of the dye laser while monitoring the wavelength with a 0.5 m focal length monochromator. An LIF spectrum is then recorded while the laser wavelength is slowly changed over a range of 0.5 - 1 nm. This fine control of the laser is accomplished by pressurizing an aluminum box which houses the laser grating up to 1300 kPa of nitrogen and then slowly bleeding the nitrogen away, changing the index of refraction. This low-tech method yields extremely linear and reproducible control of the laser wavelength. The separation between lines on the LIF spectrum can be measured accurately to $\pm 0.002 \text{ nm}$. This spectrum is then pattern-matched to the NIST line list to correctly identify the transition of interest.

Once the laser wavelength is tuned to the transition, fluorescence is collected at right angles to both laser and atomic beams through a pair of fused-silica lenses. These lenses comprise an $f/1$ optical system. Allowance is made for the insertion of optical filters between the two lenses where the fluorescence is roughly collimated. These filters can be broadband colored-glass filters or narrowband multi-layer dielectric interference filters. Their function is to block scattered laser light, light from the discharge and cascade radiation. Although cascade from higher levels is not a problem due to the selective nature of the excitation, cascade from lower-lying levels is still a possibility. Fluorescence from the beam interaction region is imaged onto the photocathode of a RCA 1P28A photomultiplier tube (PMT). The PMT signal is then recorded with a Tektronix SCD1000 transient digitizer beginning at least 7 ns after the peak of the laser pulse. This delay allows time for the complete termination of the laser so that deconvolution of the laser temporal profile from the fluorescence signal is not necessary. An average of 640 fluorescence decays is recorded. The laser wavelength is then tuned off the transition and an average of 640 background traces is recorded. These data are downloaded to a computer for analysis. The digitized data is divided into an early-time and a late-time section for analysis, each being ~ 1.5 lifetimes in length. A least-squares-fit to a single exponential is performed on the background subtracted signal to determine a lifetime in each section. Comparison of the early- and late-time lifetimes gives a quick and sensitive method to check for any systematic deviations from a clean exponential. Five such lifetime measurements are averaged together for a given set of experimental conditions. Two measurements of each lifetime are made with typically several months intervening and using a different laser transition whenever possible. This redundancy ensures that the experiment is running reproducibly, that the transitions are identified correctly in the experiment, that they are classified correctly to the upper level and that they are not masked by a hidden blend or affected by cascade radiation through lower levels.

In addition to cascade radiation, there are several other effects which must be understood and controlled to ensure a clean lifetime measurement. The dynamic range of the experiment extends from ~ 2 ns to several microseconds. The bandwidth of the PMT, digitizer and associated electronics begins to affect the fidelity of the lifetime measurements below ~ 4 ns and limits the minimum lifetime to ~ 2 ns. We assign a minimum uncertainty of 0.2 ns, such that the fractional uncertainty rises from 5% at 4 ns up to 10% at 2 ns lifetime. The other end of the dynamic range is limited by the flight-out-of-view effect, where the motion of the atoms has taken those radiating later in the decay outside the view of the PMT. This has the effect of artificially shortening the measured lifetime. This effect can be mitigated somewhat by inserting a cylindrical lens in the optical train which serves to defocus the optics in the direction of motion, making them much less sensitive to that motion. This step is taken for neutral lifetimes > 300 ns and ion lifetimes > 100 ns (ions move somewhat faster than the neutrals). It also has the unfortunate effect of diminishing the signal levels by a factor of five or so. Zeeman quantum beats arise when the atomic dipoles excited by the polarized laser have time to precess in the earth's magnetic field before they radiate. To avoid this effect, the region where the laser and atomic beams interact is placed at the center of a set of Helmholtz coils which are used to zero the field to within $\pm 2 \mu\text{T}$. This tolerance is adequate to avoid Zeeman quantum beats for shorter lifetimes, but for longer lifetimes (> 300 ns) some effect can still be observed. In these cases a high magnetic field (3 mT) is produced with a second set of coils which causes rapid precession and the Zeeman beats are washed out on the longer digitizer time windows employed. A further systematic effect arises from after-pulsing in the PMT. Generally, the characteristics of the 1P28A PMT, i.e. fast rise-time and high sensitivity in the UV and visible, are favorable for lifetime measurements. However, the PMT does produce a weak (0.1%) after-pulse as a result of the prompt electron cascade ionizing residual gas in the tube. This weak and relatively slow signal is picked up on the photocathode and results

in a systematic, reproducible lengthening of lifetimes around 100 ns. This effect of a few percent is corrected for in the final lifetimes.

We periodically measure a set of benchmark lifetimes which helps us ensure that the experiment is running reproducibly and accurately. These benchmarks are lifetimes which are well known from other sources. Some are from theoretical calculations and others from experiments which have smaller, and generally different systematic uncertainties than our own. The benchmarks measured for the current set of lifetimes are: $z^6F_{11/2}$ and $z^6D_{9/2}$ states of Fe^+ at 3.19(4) ns and 3.70(6) ns, respectively (laser-fast beam, Biémont et al. (1991)), $2^2P_{3/2}$ state of Be^+ at 8.8519(8) ns (variational method calculation, Yan et al. (1998)); the $3^2P_{3/2}$ state of neutral Na at 16.23(1) ns (NIST critical compilation of Kelleher & Podobedova (2008)); $4p'[1/2]_1$ state of Ar at 27.85(7) ns (beam-gas-laser-spectroscopy, Volz & Schmoranzler (1998)); 3^3P , 4^3P , and 5^3P states of neutral He at 94.8(1) and 219.3(2) ns (variational method calculation, Kono & Hattori (1984); Drake & Morton (2007)). These benchmarks allow us to quantify small corrections due to residual systematic effects, ensuring that our lifetimes are well within the stated uncertainty. A comparison of our lifetimes to laser-fast beam measurements performed by Scholl et al. (2002) in Sm II suggests that the stated uncertainties are conservative (Lawler et al. 2008).

3. Results and discussion

In Table 2 we report the results of lifetime measurements from this study as well as LIF results from the literature. Lifetimes measured using older, less reliable techniques are not listed. Lifetimes are given for 60 high-lying odd-parity levels of Fe I ranging in energy from 27 166.82 to 57 565.31 cm^{-1} . The fractional uncertainty in our measurements is 5%, except for those lifetimes less than 4 ns for which the absolute uncertainty is 0.2 ns. Approximately two-thirds of these lifetimes are measured for the first time. The comparison with the earlier

work is very favorable. The lifetimes in the O’Brian et al. (1991) work were measured in our (UW) lab with nearly the same apparatus as the current work (in the earlier work a different digitizer was used). We re-measured some of the original O’Brian et al. (1991) lifetimes to ensure that, even after 25 years, the experiment is giving consistent results. Happily, we see very good agreement with this older work. For eight lifetimes in common, the mean and rms differences between the current study and O’Brian et al. (1991) are -1.5% and 3.1%, respectively, using the current study as reference (in the sense (theirs – ours)/ours). The level of agreement with Engelke et al. (1993) is also very good with mean and rms differences of -1.1% and 5.4%, respectively. Our study overlaps with that of Marek et al. (1979) for only two lifetimes which agree within 0.5% for the longer lifetime around 64 ns and within 4.5% for a shorter lifetime around 9 ns. Our study overlaps with that of Langhans et al. (1995) for only two very short lifetimes less than 3 ns. We agree perfectly in one case and differ by only 0.1 ns for the other. The excellent level of agreement with these four earlier studies is typical of modern TRLIF measurements.

Measurements of branching fractions were attempted for all the transitions coming from the upper energy levels included in Table 2 and completed for 15 of them. These upper energy levels are listed in Table 3 together with their configuration, the lifetime of the level used for the determination of the $\log(gf)$ s and the completeness of each set of transitions. The remaining energy levels were excluded from our study due to the impossibility of putting the different lines onto a common intensity scale or to the presence of blended or very low signal-to-noise ratio lines. Table 4 lists the results for branching fractions, transition probabilities and $\log(gf)$ s with their uncertainties for 120 transitions of Fe I, 22 of which are new and 63 have improved uncertainties compared with existing data. The spectral lines are grouped by common upper energy level and each set is sorted in order of descending wavelength. The values of the air wavelengths, as well as the upper and lower energy levels and J were taken from Kramida et al. (2011) based on Nave et al.

(1994). In addition, the $\log(gf)$ s measured in this experiment are compared when possible with the value recommended by Fuhr and Wiese (2006), included in the last column along with the reference from the work from which the oscillator strength was taken. The letters L and P are used to indicate the method used in the O’Brian work to obtain these values and stand for ‘lifetime’ and ‘population method’, respectively.

Figs. 2 and 3 show the comparison between the new $\log(gf)$ values obtained in this experiment and those published previously, indicating if they agree within one or two σ , which represents the combined experimental uncertainty. Both plots include dashed horizontal lines indicating uncertainties of $\pm 25\%$, which correspond to values classified as ‘C’ by Fuhr and Wiese (2006), regarding their accuracy. In Fig. 2, our $\log(gf)$ s are compared to those from O’Brian et al. (1991). We have made a distinction between the $\log(gf)$ s which were obtained from measurements of lifetimes and branching fractions and those determined from extrapolated energy level populations and relative line intensities. For 13 of the compared transitions, marked in Fig. 2 by filled symbols, O’Brian et al. (1991) $\log(gf)$ s do not agree with our new values within 2σ . It is noted that only one of these values from O’Brian et al. (1991) was obtained from lifetime measurements, with the remaining 12 being determined by using the population method. Fig. 3 shows the comparison with $\log(gf)$ values from Blackwell et al. (1979, 1982a, 1982b), May et al. (1974), Bard & Kock (1994) and Banfield & Huber (1973). It is possible to see how $\log(gf)$ s from Blackwell et al. agree within 1σ with our new values, which is reassuring as their experiments are considered to be the most precise by Fuhr and Wiese (2006), with uncertainties lower than 2%. Relative $\log(gf)$ s from Blackwell et al. are claimed to be better than 2%. The comparison with $\log(gf)$ s from May et al. (1974), obtained from emission measurements from a wall-stabilized arc, shows a wider scatter, which is not strange given the large uncertainties assigned by Fuhr and Wiese (2006). The only $\log(gf)$ value from Bard & Kock (1994) available for comparison shows a good agreement within

1σ , whereas the $\log(gf)$ from Banfield & Huber (1973) differs significantly from our value, although the difference lies within 2σ .

4. Solar spectral synthesis

A subset of the new gf -values measured in this work were used to determine iron line abundances from the solar spectrum obtained with the Kitt Peak Fourier Transform Spectrometer by Kurucz et al. (1984). The high-quality observations and the well-known atmospheric parameters available for the Sun make it an ideal test case to evaluate the impact of new atomic data on stellar spectral synthesis. We selected 17 lines from Table 4 which show low contamination from blends at the spectral resolution of the solar flux atlas, and which are located in regions of good continuum placement. The observed spectrum has a minimum wavelength of 300 nm, and it is very crowded at wavelengths below ~ 400 nm, which excludes about two thirds of the lines published in this work. Among the remaining lines, about half were too blended to attempt any abundance derivation. The selected lines are listed in Table 5 together with the required input atomic data in columns 1 to 4 (central wavelength, lower level energy E_{low} , gf -value, and van der Waals parameter). The latter is used to account for line broadening due to collisions with neutral hydrogen and was extracted from the VALD database (Kupka et al. 1999, Heiter et al. 2008). The meaning of the values for the van der Waals broadening parameter given in Table 5 (column 3) is as follows. Values greater than zero were obtained from Anstee, Barklem & O’Mara (ABO) theory (Anstee & O’Mara 1991, Anstee & O’Mara 1995, Barklem et al. 2000) and are expressed in a packed notation where the integer component is the broadening cross-section, σ , in atomic units, and the decimal component is the dimensionless velocity parameter, α . Values less than zero are the log of the broadening parameter, γ_6 (rad s^{-1}), per unit perturber number density, N (cm^{-3}), at 10 000 K (i.e. $\log[\gamma_6/N]$ in units of $\text{rad s}^{-1} \text{cm}^3$)

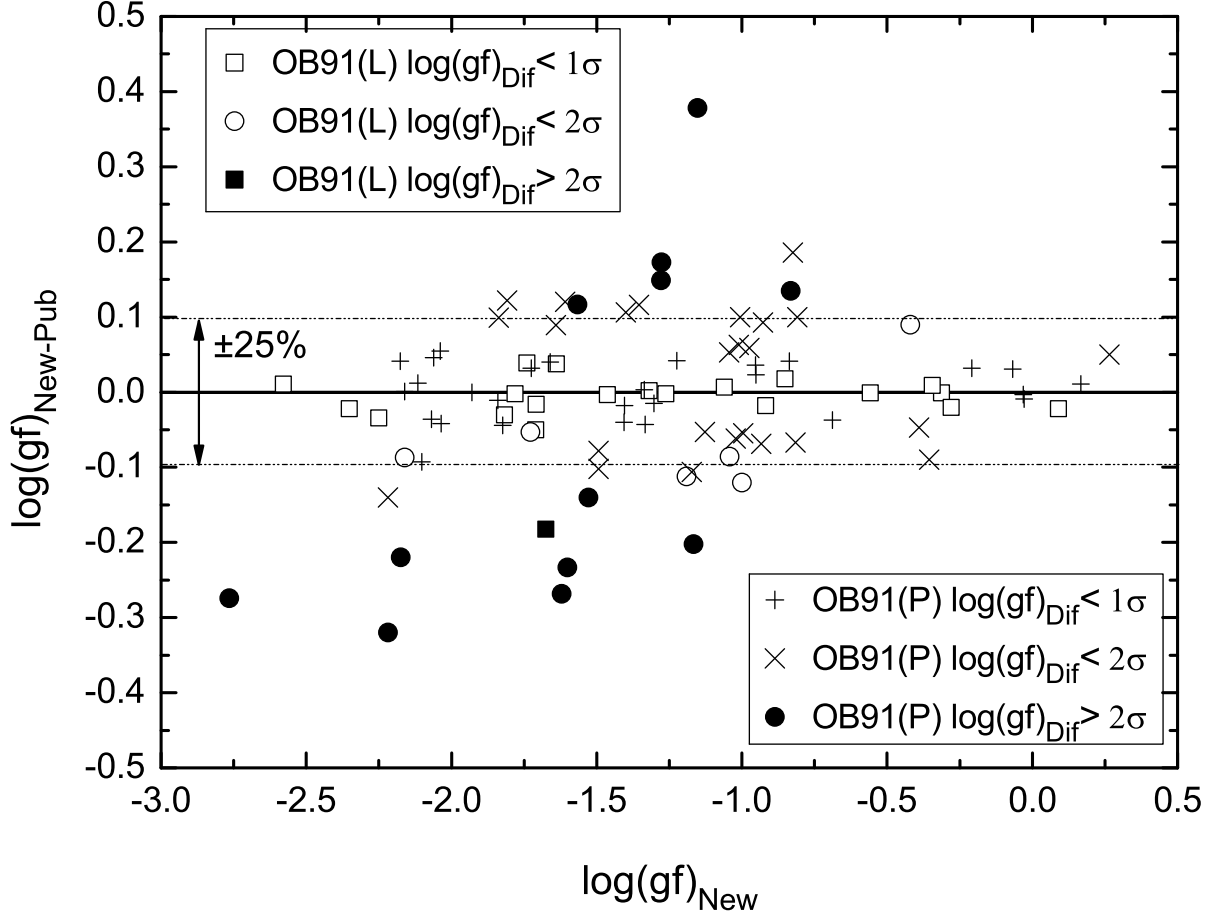


Fig. 2.— Comparison of the new $\log(gf)$ values measured in this work with those of O’Brian et al. (1991) obtained from lifetimes (L) and extrapolating energy level populations (P). The solid horizontal line represents perfect agreement between the two sets of values. The dashed horizontal line indicates uncertainties of $\pm 25\%$, coded as ‘C’ by Fuhr and Wiese (2006). Agreement within the combined experimental uncertainty is indicated by $< 1\sigma$.

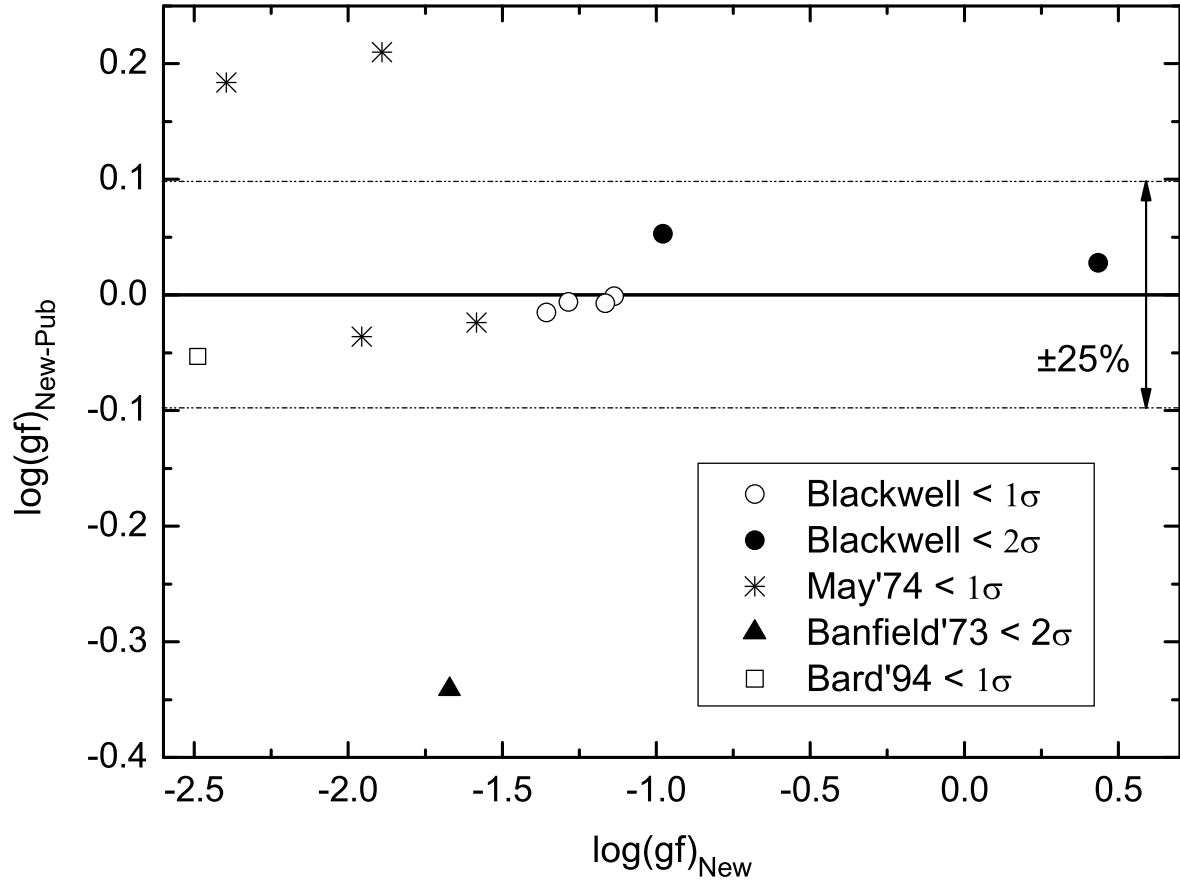


Fig. 3.— Comparison between our new oscillator strengths and those from Blackwell et al. (1979, 1982a, 1982b), May et al. (1974), Bard & Kock (1994) and Banfield & Huber (1973). Close agreement with Blackwell et al. is used as an indication of the quality of our new data.

from Kurucz (2014). These were used only when ABO data were unavailable. See Gray (2005) for more details.

The spectral synthesis was done with the one-dimensional, plane-parallel radiative transfer code SME (Valenti & Piskunov 1996, Piskunov & Valenti 2017, version 531) assuming local thermodynamic equilibrium (LTE) and using a model atmosphere interpolated in the MARCS grid included in the SME distribution (Gustafsson et al. 2008). We adopted an effective temperature of 5772 K and a logarithmic surface gravity (cm s^{-2}) of 4.44 (Heiter et al. 2015a, Pršat et al. 2016), a microturbulence of 1.0 km s^{-1} and a projected rotational velocity of $v_{\text{rot}}\sin(i) = 1.6 \text{ km s}^{-1}$ (Valenti & Piskunov 1996). The instrumental profile was assumed to be Gaussian, with a width corresponding to the spectral resolution of the observations ($R=200\,000$). Each line profile was fitted individually using χ^2 -minimization between observed and synthetic spectra while varying the iron abundance and the macroturbulence broadening, parameterised by a velocity v_{macro} in the radial-tangential model (Gray 2005). In addition, a small radial velocity correction was applied to each line, allowing for variations in the wavelength scale of the observations. For each line we determined the region of the line profile which seemed to be free from blends in the observed spectrum, and only spectrum points within that region were used to calculate the χ^2 .

The results are given in Table 5, where we list the best-fit iron abundance $\log(\varepsilon)$ for each line (column 10) on the standard astronomical scale¹. We also list the v_{macro} values derived for each line (column 9), as well as a measure for the goodness of fit (RMS deviation, column 11), ranging from 0.4 to 1.9 percent. The largest deviations are found for lines at wavelengths at or below 450 nm, and the smallest RMS values for lines above 700 nm. Most

¹ $\log(\varepsilon) = \log_{10}(N_{\text{Fe}}/N_{\text{H}}) + 12$, where N_{Fe} and N_{H} are the number densities of iron and hydrogen atoms, respectively.

of the abundances fall in the range from 7.3 to 7.6, with associated macroturbulence values between 2.5 and 3.7 km s⁻¹ and radial velocity corrections of 0.2 to 0.4 km s⁻¹. However, the line at 4709 Å has $v_{\text{macro}} \gtrsim 4$ and an abundance of 7.9, significantly higher than the above range. This indicates contamination by undetected blends that have not been taken into account in the fit. Excluding this line, the mean abundance and standard deviation are $\log(\varepsilon)_{\text{new}} = 7.47 \pm 0.10 \text{ dex}^2$ (16 lines), which is similar to the values found in the previous two papers in this series (7.44 ± 0.08 dex in Ruffoni et al. 2014 and 7.45 ± 0.06 dex in Den Hartog et al. 2014), and agrees with recent publications, such as 7.43 ± 0.05 from Bergemann et al. (2012) (MARCS LTE result), and 7.40 ± 0.04 from Scott et al. (2015) (mean of MARCS LTE abundances in their Table 1).

The line-to-line abundance scatter might be influenced by non-LTE effects, which are however expected to be small in solar-like atmospheres. Unfortunately non-LTE corrections have only been published for few of the lines analysed here. Four of the lines were investigated by Gehren et al. (2001), who derived non-LTE–LTE abundance differences of 0.03 dex for the 4495 and 5380 Å lines, 0.05 dex for 4448 Å, and –0.11 dex for 4433 Å. Applying these corrections would lead to a slightly larger scatter. On the other hand, the more recent calculations by Bergemann et al. (2012) and Lind et al. (2012), made available through the INSPECT database³ include two of the lines (4495, 5380 Å), both with non-LTE corrections of 0.01 dex. If similar corrections apply to the remaining lines then they do not have any impact on the abundance scatter derived here.

We repeated the abundance determination for the same set of lines using the best previously published experimental or theoretical $\log(gf)$ values (see Table 5 for values and references, in columns 6 to 8, and for results in columns 12 and 13). The regions of the line

²The unit dex stands for decimal exponent, $x \text{ dex} = 10^x$.

³<http://www.inspect-stars.com>

profiles used for the fit were the same as above, and the macroturbulence values were those derived in the analysis with the new $\log(gf)$ values⁴ The results for both the previously published data and the new data are illustrated in Fig. 4. The differences in derived abundances are consistent with the differences in $\log(gf)$, and are larger than 0.05 dex for six lines⁵. The mean abundance and standard deviation for previous data including the same 16 lines as above are $\log(\varepsilon)_{\text{pub}} = 7.52 \pm 0.13$ dex, which is close to $\log(\varepsilon)_{\text{new}}$, although slightly offset towards higher abundances and with a somewhat larger scatter. In summary, the small scatter in the line abundances derived with the new data, and the satisfactory agreement with recently published values for the solar iron abundance validates the general accuracy of the new measurements.

5. Conclusions

We report radiative lifetimes for 60 odd-parity energy levels ranging from 27 166 to 57 562 cm^{-1} , 39 of which had not been measured before. The uncertainties for these lifetimes are the larger of $\pm 5\%$ or 0.2 ns. When values are available in the literature, our results are in good agreement with them.

We provide 120 experimental $\log(gf)$ values (transition probabilities) for Fe I transitions within the spectral range 213-1033 nm coming from 16 upper energy levels, 24 of which had no previous experimental data. The uncertainty of these oscillator strengths has been carefully calculated and it ranges between 0.02 dex for the strongest lines and 0.09 dex for the very weak ones. This accuracy is an improvement over previous $\log(gf)$ measurements

⁴Simultaneous variation of macroturbulence resulted in the same v_{macro} values, except for two lines: 5533 Å, and 7308 Å, with 7%, and 9% lower values, respectively.

⁵4548, 5380, 5533, 7220, 7308, 7443 Å.

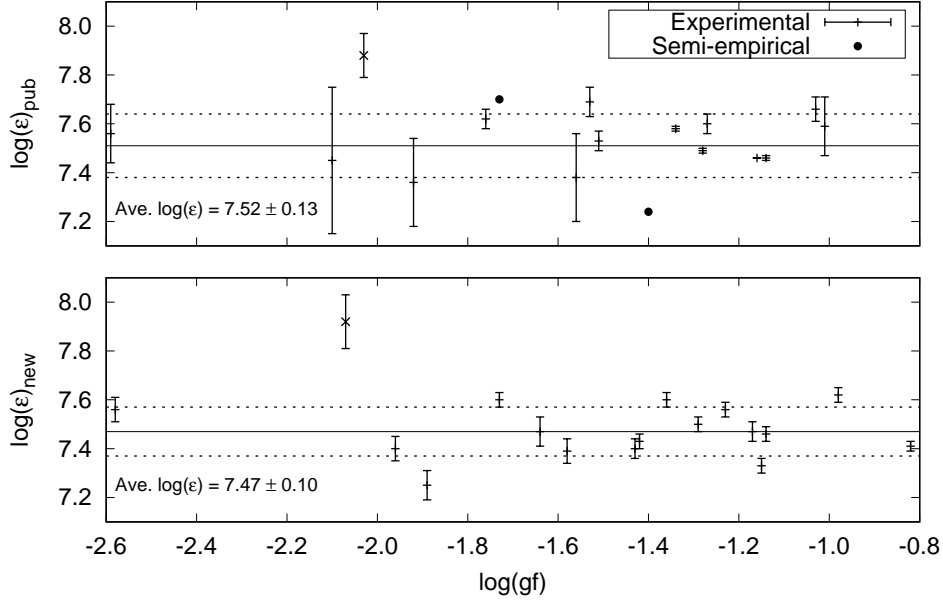


Fig. 4.— Solar iron abundance, $\log(\epsilon)$, obtained from the synthesis of individual lines listed in Table 5 using the $\log(gf)$ values from this work, $\log(gf)_{\text{new}}$ (lower panel), and the best previously published values, $\log(gf)_{\text{pub}}$ (upper panel). The point in each panel marked with a cross may be affected by undetected blends (see text) and was excluded from the calculation of the average $\log(\epsilon)$. The solid and dotted horizontal lines in each panel indicate the unweighted average abundance and the standard deviation, respectively. The error bars indicate only the uncertainty of the experimental gf -values (columns 5 and 7 in Table 5) and do not capture the uncertainties associated with the solar atmospheric modeling and spectral synthesis.

for around 72 of the transitions, making our new $\log(gf)$ values good candidates for use in the analysis of stellar spectra and the determination of chemical abundances. Our $\log(gf)$ results are in good agreement with those of Blackwell et al. (1979, 1982a, 1982b) and in general with O’Brian et al. (1991) data.

Acknowledgements

MTB, JCP and MPR would like to thank the UK Science and Technology Facilities Council (STFC) for support under research grant ST/N000838/1. EADH, JEL and AG would like to acknowledge funding from the National Science Foundation through award AST-1211055 and through the NSF REU program award AST-0907732. U.H. acknowledges support from the Swedish National Space Board (SNSB/Rymdstyrelsen). This work has made use of the VALD database, operated at Uppsala University, the Institute of Astronomy RAS in Moscow, and the University of Vienna. This work has made use of the NSO/Kitt Peak FTS data, produced by NSF/NOAO.

REFERENCES

- Anstee, S.D. & O'Mara, B.J., 1991, MNRAS, 253, 549
- Anstee, S.D. & O'Mara, B.J., 1995, MNRAS, 276, 859
- Banfield, F. P. & Huber, M. C. E., 1973, *Astrophys. J.*, 186, 335
- Bard, A. & Kock, M., 1994, *Astron. Astrophys.*, 282, 1014
- Barklem, P. S., Piskunov, N. & O'Mara, B. J., 2000, *Astron. and Astrophys. Suppl. Ser.*, 142, 467, (BPM)
- Bergemann, M., Lind, K., Collet, R., Magic, Z. & Asplund M., 2012, MNRAS, 427, 27
- Biémont, E., Baudoux, M., Kurucz, R. L., Ansbacher, W., & Pinnington, E. H. 1991, *A&Ap*, 249, 539
- Bigot, L. & Thévenin, F., 2006, MNRAS, 372, 609
- Blackwell, D. E., Booth, A. J., Haddock, D. J., Petford, A. D., & Leggett, S. K., 1986, MNRAS, 220, 549
- Blackwell, D. E., Ibbetson, P. A., Petford, A. D., & Shallis, M. J., 1979a, MNRAS, 186, 633
- Blackwell, D. E., Petford, A. D., & Shallis, M. J. 1979b, MNRAS, 186, 657
- Blackwell, D. E., Petford, A. D., Shallis, M. J., & Simmons, G. J. 1980, MNRAS, 191, 445
- Blackwell, D. E., Petford, A. D., Shallis, M. J., & Simmons, G. J., 1982a, MNRAS, 199, 43
- Blackwell, D. E., Petford, A. D., & Simmons, G. J. 1982b, MNRAS, 201, 595
- Den Hartog, E.A., Ruffoni, M.P., Lawler, J.E., Pickering, J.C., Lind, K. & Brewer, N.R., 2014, *ApJS*, 215, 23

- Drake, G. W. F. & Morton, D. C., 2007, *ApJS*, 170, 251
- Engelke, D., Bard, A. & Kock, M., 1993, *Z. Phys. D*, 27, 325
- Fuhr, J. R. & Wiese, W. L., 2006, *J. Phys. Chem. Ref. Data*, 35, 1669
- Gehren, T., Korn, A. J. & Shi, J., 2001, *A&A*, 380, 645
- Gilmore, G., Randich, S., Asplund, M., et al., 2012, *Messenger*, 147, 25
- Gray, D. F., 2005, “The Observation and Analysis of Stellar Photospheres” 3rd Ed., Chapter 11 (Cambridge, UK: Cambridge University Press)
- Gustafsson, B., Edvardsson, B., Eriksson, K., Jørgensen, U. G., Nordlund, Å. & Plez B., 2008, *Astron. Astrophys.*, 486, 951
- Heiter, U., Barklem, P., Fossati, L., et al., 2008, *Journal of Physics Conference Series*, 130, 012011
- Heiter, U., Jofré, P., Gustafsson, B., et al., 2015a, *A&A*, 582, A49
- Heiter, U., Lind, K., Asplund, M., et al., 2015b, *Phys. Scr.*, 90, 054010
- Huber, M. C. E. & Sandeman, R. J., 1986, *Rep. Prog. Phys.*, 49, 397
- Katz, D., Munari, U., Cropper, M., Zwitter, T., Thévenin, F., David, M., et al., 2004, *MNRAS*, 354, 1223
- Kelleher, D. E. & Podobedova, L. I., 2008, *J. Phys. Chem. Ref. Data*, 37, 267
- Kono, A. & Hattori, S., 1984, *Phys. Rev. A*, 29, 2981
- Kramida, A., Ralchenko, Yu., Reader, J., & NIST ASD Team (2011). NIST Atomic Spectra Database (ver. 4.0.1), [Online]. Available: <http://physics.nist.gov/asd> [2011, April]. National Institute of Standards and Technology, Gaithersburg, MD

- Kupka, F., Piskunov, N., Ryabchikova, T. A., Stempels, H. C. & Weiss, W. W., 1999, A&AS, 138, 119
- Kurucz, R. L., Furenlid, I., Brault, J. & Testerman, L., 1984, “Solar flux atlas from 296 to 1300 nm”, National Solar Observatory Atlas (Sunspot, NM: National Solar Observatory)
- Kurucz, R. L., 2007, <http://kurucz.harvard.edu/atoms/2700/>
- Kurucz, R. L., 2014, on-line database of observed and predicted atomic transitions, <http://kurucz.harvard.edu/atoms/2600/>
- Langhans, G., Schade, W. & Helbig, V. 1995, Z. Phys. D 34, 151
- Lawler, J. E., Den Hartog, E. A., Sneden, C. & Cowan, J. J., 2008, Can. J. Phys., 86, 1033
- Lind, K., Bergemann, M. & Asplund, M., 2012, MNRAS, 427, 50
- Marek, J., Richter, J. & Stahnke, H. J., 1979, Phys. Scr., 19, 325
- May, M., Richter, J. & Wichelmann, J., 1974, Astron. Astroph. Suppl. Ser., 18, 405
- Nave, G., Johansson, S., Learner, R. C. M., Thorne, A. P. & Brault, J. W., 1994, ApJS, 94, 221
- Nave, G., Sansonetti, C. J. & Griesmann, U., 1997, in OSA Technical Digest Ser. Vol. 3, Fourier Transform Spectroscopy, Optical Society of America, Washington DC, p. 38
- Nave, G. & Johansson, S., 2013, ApJS, 204, 1
- O’Brian, T. R., Wickliffe, M. E., Lawler, J. E., Whaling, W., Brault & J. W., 1991, J. Opt. Soc. Am. B, 8, 1185

- Perryman, M. A. C., de Boer, K. S., Gilmore, G., Høg, E., Lattanzi, M. G., Lindegren, L., Luri, X., Mignard, F., Pace, O. & de Zeeuw, P. T., 2001, *A & A*, 369, 339
- Pickering, J. C., Johansson, S. & Smith P. L., 2001a, *A & A*, 377, 361
- Pickering, J. C., Thorne, A. P. & Perez R., 2001b, *ApJS*, 132, 403
- Pickering, J. C., Blackwell-Whitehead, R., Thorne, A. P., Ruffoni, M.P. & Holmes, C.E., 2011, *Can. J. Phys.*, 89, 387
- Piskunov, N. & Valenti, J. A., 2017, *A&A*, 597, A16
- Pršat, A., Harmanec, P., Torres, G., et al., 2016, *AJ*, 152, 41
- Ruffoni, M. P., Allende-Prieto, C., Nave, G. & Pickering, J. C. 2013a, *ApJ*, 779, 17
- Ruffoni, M. P., 2013b, *Comp. Phys. Comm.*, 184, 1770
- Ruffoni, M. P., Den Hartog, E. A., Lawler, J. E., Brewer, N. R., Lind, K., Nave, G. & Pickering, J. C., 2014, *MNRAS*, 441, 3127
- Scholl, T. J., Holt, R. A., Masterman, D., Rivest, R. C., Rosner, S. D., & Sharikova, A., 2002, *Can. J. Phys.*, 80, 1621
- Scott, P., Asplund, M., Grevesse, N., Bergemann, M., & Sauval, A. J., 2015, *A&A*, 573, A26
- Thorne, A. P., Harris C. J., Wynne-Jones, I., Learner, R. C. M. & Cox, G., 1987, *J. Phys.* E, 20, 54
- Thorne, A. P., 1996, *Phys. Scripta*, T65, 31
- Thorne, A. P., Litzén, U. & Johansson, S., 2007, in “Spectrophysics: Principles and Applications” 3rd Ed., Chapter 7.7

U.S. Naval Observatory & Royal Greenwich Observatory, “The Astronomical Almanac for the year 2014”, 2013, Washington: U.S. Government Printing Office (USGPO) and London: The Stationery Office

Valenti, J. A. & Piskunov, N., 1996, *Astron. Astrophys. Suppl. Ser.*, 118, 595

Volz, U. & Schmoranzler, H., 1998, in *AIP Conf. Proc.* 434, “Atomic and Molecular Data and Their Applications”, ed. P. J. Mohr and W. L. Wiese, Woodbury, NY:AIP, 67

Wiese, W. L. & Kelleher, D. E., 1998, *The Critical Assesment of Atomic Transition Probabilities, Atomic and Molec. Data and their appl.*, (ed. Mohr & Wiese).

Yan, Z.-C., Tambasco, M. & Drake, G. W. F., 1998, *Phys. Rev. A*, 57, 1652

Table 1. FTS spectra used for the branching fraction measurements.

Spectrum	Wavenumber range used (cm^{-1})	Resolution (cm^{-1})	Detector	Filter	P gas (mbar)	I lamp (mA)	Spectrum filename ^a
A (NIST)	9600 – 26000	0.02	Si diode	None	2.1	2000	Fe0301to0403_Calib
B (IC)	21000 – 33000	0.037	R11568 PMT	Schott BG3	1.3	700	F130610.002.047_Scaled
C (IC)	23000 – 41000	0.037	R11568 PMT	UG5	1.4	700	Fe130624.011.039_Scaled
D (IC)	31000 – 47000	0.037	R7154 PMT	None	1.3	1000	Fe130603.021.059_Calib
G (IC)	20000 – 35000	0.037	R11568 PMT	Schott BG3	1.3	1000	Fe130604A.007.034

^aSeveral spectra were coadded to improve the signal-to-noise ratio of the spectral lines.

Table 2. Radiative lifetimes of Fe I odd-parity levels including many higher levels studied for the first time in our work. The uncertainty in our measurements is the larger of $\pm 5\%$ or ± 0.2 ns

Configuration ^a	Term ^a	J	Level ^a (cm ⁻¹)	Laser Wavelengths ^a (nm)	Lifetime (ns)	
					This Expt.	Other Expt.
3d ⁶ (⁵ D)4s4p(³ P ^o)	z ⁵ F ^o	4	27166.82	505.1634, 514.2928	63.4	63.6 ^b , 66.6 ^c , 63.7(4.0) ^d
3d ⁶ (⁵ D)4s4p(³ P ^o)	z ⁵ P ^o	3	29056.324	344.0605, 349.0573	43.7	
3d ⁶ (⁵ D)4s4p(³ P ^o)	z ⁵ P ^o	2	29469.024	344.0988, 347.5449	43.2	
3d ⁶ (⁵ D)4s4p(³ P ^o)	z ⁵ P ^o	1	29732.736	344.3876, 347.6701	42.6	
3d ⁷ (⁴ F)4p	z ⁵ G ^o	6	34843.957	358.1192	9.2	9.6(0.6) ^d
3d ⁶ (⁵ D)4s4p(¹ P ^o)	x ⁵ D ^o	3	39969.853	250.1131, 445.9117	2.7	2.6 ^b , 2.8 ^c , 2.7(1) ^e
3d ⁶ (⁵ D)4s4p(¹ P ^o)	x ⁵ D ^o	1	40404.518	251.8101, 444.7716	2.8	2.6 ^b , 2.9 ^c , 2.7(1) ^e
3d ⁵ (⁶ S)4s ² 4p	y ⁷ P ^o	4	40421.938	247.3156	317	309 ^b
3d ⁶ (³ F ₂)4s4p(³ P ^o)	v ⁵ D ^o	4	44022.525	227.0862, 229.2524	96.5	95.9 ^b
3d ⁶ (³ F ₂)4s4p(³ P ^o)	v ⁵ D ^o	1	44760.746	226.9098, 228.3303	21.3	21.4 ^b
3d ⁶ (³ F ₂)4s4p(³ P ^o)	w ⁵ F ^o	4	44415.074	225.0790, 227.2069	41.6	41.2 ^b
3d ⁷ (⁴ P)4p	y ⁵ S ^o	2	44511.812	226.7084, 273.6963	13.3	13.6 ^b
3d ⁷ (⁴ P)4p	w ⁵ P ^o	3	46137.097	216.6773, 218.6486	3.2	
3d ⁷ (⁴ P)4p	w ⁵ P ^o	2	46313.537	219.1839, 220.0724	3.2	
3d ⁷ (⁴ P)4p	w ⁵ P ^o	1	46410.381	218.7194, 219.6041	3.5	
3d ⁶ (³ P ₂)4s4p(³ P ^o)	z ³ S ^o	1	46600.818	218.6892, 219.1204	16.5	
3d ⁶ (³ P ₂)4s4p(³ P ^o)	y ³ P ^o	2	46727.074	215.8629, 344.7277	19	
3d ⁶ (³ P ₂)4s4p(³ P ^o)	y ³ P ^o	1	46901.832	217.2584, 217.6840	11	
3d ⁷ (⁴ P)4p	u ⁵ D ^o	4	46720.842	213.9697, 215.8919	12.2	
3d ⁷ (⁴ P)4p	u ⁵ D ^o	3	46744.993	215.7794, 217.1296	9.9	

Table 2—Continued

Configuration ^a	Term ^a	J	Level ^a (cm ⁻¹)	Laser Wavelengths ^a (nm)	Lifetime (ns)	
					This Expt.	Other Expt.
3d ⁷ (⁴ P)4p	u ⁵ D ^o	2	46888.517	216.4548, 217.3213	11.4	
3d ⁷ (⁴ P)4p	u ⁵ D ^o	0	47171.531	215.9923, 341.8507	7.8	
3d ⁷ (⁴ P)4p	u ⁵ D ^o	1	47177.234	216.3862, 341.7840	9.8	9.3 ^c
3d ⁶ (³ F ₂)4s4p(³ P ^o)	x ³ F ^o	4	46889.142	213.2016, 250.1693	11.1	10.7 ^c
3d ⁶ (³ F ₂)4s4p(³ P ^o)	x ³ F ^o	3	47092.712	214.1718, 215.5019	18.2	17.4 ^c
3d ⁶ (³ F ₂)4s4p(³ P ^o)	x ³ F ^o	2	47197.01	215.0184, 215.8734	22.9	21.8 ^c
3d ⁷ (⁴ P)4p	w ³ D ^o	3	47017.188	214.5189, 215.8534	11.6	11.5 ^c
3d ⁷ (⁴ P)4p	w ³ D ^o	2	47136.084	215.3006, 216.1579	11.9	11.7 ^c
3d ⁷ (⁴ P)4p	w ³ D ^o	1	47272.027	214.6720, 215.5243	14.2	15.1 ^c
3d ⁶ (³ P ₂)4s4p(³ P ^o)	¹ D ^o	2	47419.687	213.9934, 214.8403	33	
3d ⁷ (² G)4p	z ¹ G ^o	4	47452.717	251.6570, 388.4358	66.2	59.7 ^c
3d ⁶ (³ G)4s4p(³ P ^o)	v ⁵ F ^o	5	47606.114	245.7596, 386.1343	27.8	
3d ⁶ (³ G)4s4p(³ P ^o)	v ⁵ F ^o	4	47929.997	246.5149, 248.6691	16.8	
3d ⁶ (³ G)4s4p(³ P ^o)	v ⁵ F ^o	3	48122.928	245.3475, 247.4814	12.9	
3d ⁶ (³ G)4s4p(³ P ^o)	v ⁵ F ^o	2	48238.847	209.0383, 248.3533	11.2	11.2 ^c
3d ⁶ (³ G)4s4p(³ P ^o)	v ⁵ F ^o	1	48350.606	247.6656, 248.7065	11.2	
3d ⁵ (⁶ S)4s ² 4p	v ⁵ P ^o	3	47966.585	208.4121, 210.2353	6.3	
3d ⁵ (⁶ S)4s ² 4p	v ⁵ P ^o	2	48163.446	209.3684, 210.6394	6.4	
3d ⁵ (⁶ S)4s ² 4p	v ⁵ P ^o	1	48289.871	210.0797, 210.8958	5.9	
3d ⁷ (⁴ P)4p	x ³ P ^o	2	48304.643	208.7510, 210.8301	12.7	
3d ⁷ (⁴ P)4p	x ³ P ^o	1	48516.138	209.8938, 210.2910	10.7	10.6 ^c
3d ⁷ (² G)4p	z ¹ H ^o	5	48382.603	412.0206, 419.9094	16.2	

Table 2—Continued

Configuration ^a	Term ^a	J	Level ^a (cm ⁻¹)	Laser Wavelengths ^a (nm)	Lifetime (ns)	
					This Expt.	Other Expt.
3d ⁷ (² G)4p	w ³ F ^o	4	49108.896	239.5505, 269.2248	16.7	
3d ⁷ (² G)4p	w ³ F ^o	3	49242.886	366.952	18.7	
3d ⁷ (² G)4p	w ³ F ^o	2	49433.131	367.7627	12.8	
3d ⁷ (² G)4p	z ¹ F ^o	3	50586.878	384.3256	18.5	
3d ⁶ (⁵ D)4s(⁶ D)5p	u ⁵ F ^o	5	51016.66	226.7469	20.6	
3d ⁶ (⁵ D)4s(⁶ D)5p	u ⁵ F ^o	4	51381.457	224.8860, 227.1782	21.8	
3d ⁶ (⁵ D)4s(⁶ D)5p	t ⁵ D ^o	4	51076.628	226.4389, 228.7631	16.4	
3d ⁷ (² H)4p	u ³ G ^o	5	51373.91	253.7458, 337.0783	14.5	15.4 ^c
3d ⁷ (² H)4p	u ³ G ^o	4	51668.186	311.9494, 336.9547	15.2	13.5 ^c
3d ⁷ (⁴ F)5p	⁵ G ^o	6	53069.357	216.6585	55.5	
3d ⁷ (⁴ F)5p	⁵ G ^o	4	53852.114	216.7386, 238.7282	30.3	
3d ⁷ (⁴ F)5p	⁵ F ^o	5	53084.789	216.5861	25.5	
3d ⁷ (⁴ F)5p	⁵ F ^o	4	53388.637	215.1695, 217.2670	21.9	
3d ⁷ (² H)4p	¹ I ^o	6	53093.529	373.8304, 411.8544	10.6	
3d ⁷ (⁴ F)5p	³ F ^o	3	54289.034	213.0965, 214.7045	19.8	
3d ⁶ (³ D)4s4p(³ P ^o)	⁵ D ^o	1	53975.744	218.1721, 277.3232	18.2	
3d ⁶ (³ D)4s4p(³ P ^o)	⁵ D ^o	4	54301.34	211.0235, 272.0196	19	
3d ⁶ (³ P ₂)4s4p(¹ P ^o)	³ D ^o	3	57565.305	219.2823, 255.1093	6.3	

^aConfigurations, terms, level energies, and Ritz wavelengths are from the NIST Atomic Spectra Database (<http://www.nist.gov/pml/data/asd.cfm>).

^bO'Brian et al. (1991) TR-LIF with uncertainties equal to the larger of $\pm 5\%$ or ± 0.2 ns.

^cLanghans et al. (1995) TR-LIF with uncertainties of $\pm 10\%$ for lifetimes < 3 ns and $\pm 5\%$ for the remainder.

^dMarek et al. (1979) delayed coincidence after laser excitation.

^eLanghans et al. (1995)

Table 3. Completeness of the set of transitions from each upper level estimated by using the calculated branching fractions of Kurucz (2007).

Energy level (cm ⁻¹) ^a	Configuration level ^a	Lifetime used (ns) ^b	Completeness (%) ^c
34843.957	3d ⁷ (⁴ F)4p z ⁵ G ^o	9.2	100
39969.853	3d ⁶ (⁵ D)4s4p(¹ P ^o) x ⁵ D ^o	2.7	99
40404.518	3d ⁶ (⁵ D)4s4p(¹ P ^o) x ⁵ D ^o	2.8	99
44022.525	3d ⁶ (³ F ₂)4s4p(³ P ^o) v ⁵ D ^o	96.5	99
44415.074	3d ⁶ (³ F ₂)4s4p(³ P ^o) w ⁵ F ^o	41.6	99
44760.746	3d ⁶ (³ F ₂)4s4p(³ P ^o) v ⁵ D ^o	21.3	98
46720.842	3d ⁷ (⁴ P)4p u ⁵ D ^o	12.2	98
46889.142	3d ⁶ (³ F ₂)4s4p(³ P ^o) x ³ F ^o	11.1	91
47092.712	3d ⁶ (³ F ₂)4s4p(³ P ^o) x ³ F ^o	18.2	96
47197.010	3d ⁶ (³ F ₂)4s4p(³ P ^o) x ³ F ^o	22.9	82
48350.606	3d ⁶ (³ G)4s4p(³ P ^o) v ⁵ F ^o	11.2	94
48382.603	3d ⁷ (² G)4p z ¹ H ^o	16.2	99
50586.878	3d ⁷ (² G)4p z ¹ F ^o	18.5	94
51373.910	3d ⁷ (² H)4p u ³ G ^o	14.5	94
53093.529	3d ⁷ (² H)4p ¹ I ^o	10.6	98

^aThe energy and configuration levels are taken from Kramida et al. (2011).

^bExperimental lifetimes measured in this work. The uncertainty of these values is the larger of $\pm 5\%$ or ± 0.2 ns.

^cCompleteness of the set of transitions from each upper energy level estimated as described in Pickering et al. (2001a) and Pickering et al. (2001b) by using the calculated branching fractions of Kurucz (2007).

Table 4. Experimental BFs, transition probabilities and $\log(gf)$ values for 16 odd-parity energy levels of Fe I.

Wavelength ^a (nm)	Upper Level ^a		Lower Level ^a		BF ^b	U_{BF} ^b (%)	A_{ul} ^c (10^6 s^{-1})	This experiment ^d $\log(gf)$	Published ^e	
	$E \text{ (cm}^{-1}\text{)}$	J	$E \text{ (cm}^{-1}\text{)}$	J					$\log(gf)$	Ref.
358.1193	34843.957	6	6928.268	5	1.0000	0.00	108.70 (5)	0.43 ± 0.02	0.406 ± 0.005	BL79
463.0120	39969.853	3	18378.185	2	0.0003	11.9	0.12 (13)	-2.58 ± 0.05	-2.59 ± 0.12	OB91 L
449.4563	39969.853	3	17726.987	2	0.0090	3.4	3.44 (6)	-1.14 ± 0.03	-1.14 ± 0.01	BL82a
445.9117	39969.853	3	17550.180	3	0.0065	3.2	2.49 (6)	-1.29 ± 0.03	-1.28 ± 0.01	BL82a
312.5651	39969.853	3	7985.784	2	0.0049	7.5	1.90 (9)	-1.71 ± 0.04	-1.66 ± 0.08	OB91 L
310.0665	39969.853	3	7728.059	3	0.0362	5.9	13.94 (8)	-0.85 ± 0.03	-0.87 ± 0.08	OB91 L
306.7244	39969.853	3	7376.764	4	0.0999	5.6	38.42 (8)	-0.42 ± 0.03	-0.51 ± 0.07	OB91 L
254.5978	39969.853	3	704.007	2	0.1858	5.1	71.44 (7)	-0.31 ± 0.03	-0.31 ± 0.05	OB91 L
252.7435	39969.853	3	415.933	3	0.4774	3.1	183.63 (6)	0.090 ± 0.03	0.11 ± 0.04	OB91 L
250.1132	39969.853	3	0.000	4	0.1794	5.2	69.00 (7)	-0.34 ± 0.03	-0.35 ± 0.05	OB91 L
444.7717	40404.518	1	17927.381	1	0.0138	4.0	4.94 (6)	-1.36 ± 0.03	-1.34 ± 0.01	BL82a
440.8414	40404.518	1	17726.987	2	0.0058	5.5	2.08 (8)	-1.74 ± 0.03	-1.78 ± 0.12	OB91 L
309.9895	40404.518	1	8154.713	1	0.0417	6.0	14.91 (8)	-1.19 ± 0.03	-1.08 ± 0.05	OB91 L
308.3741	40404.518	1	7985.784	2	0.0655	5.9	23.41 (8)	-1.00 ± 0.03	-0.88 ± 0.05	OB91 L
253.5607	40404.518	1	978.074	0	0.2678	4.7	95.63 (7)	-0.56 ± 0.03	-0.56 ± 0.04	OB91 L
252.9835	40404.518	1	888.132	1	0.0881	6.9	31.48 (9)	-1.04 ± 0.04	-0.96 ± 0.04	OB91 L
251.8102	40404.518	1	704.007	2	0.5167	2.9	184.54 (6)	-0.28 ± 0.02	-0.26 ± 0.03	OB91 L
377.6455	44022.525	4	17550.180	3	0.1061	3.8	1.10 (6)	-1.68 ± 0.03	-1.49 ± 0.05	OB91 L
275.4427	44022.525	4	7728.059	3	0.1559	4.8	1.62 (7)	-1.78 ± 0.03	-1.78 ± 0.03	OB91 L
272.8021	44022.525	4	7376.764	4	0.3310	3.8	3.43 (6)	-1.46 ± 0.03	-1.46 ± 0.03	OB91 L
269.5036	44022.525	4	6928.268	5	0.0438	5.5	0.45 (8)	-2.35 ± 0.03	-2.33 ± 0.03	OB91 L
229.2525	44022.525	4	415.933	3	0.3122	4.0	3.24 (6)	-1.64 ± 0.03	-1.68 ± 0.03	OB91 L
227.0863	44022.525	4	0.000	4	0.0484	6.0	0.50 (8)	-2.46 ± 0.03		
372.1272	44415.074	4	17550.180	3	0.0339	15.3	0.81 (16)	-1.82 ± 0.07	-1.79 ± 0.05	OB91 L
272.4953	44415.074	4	7728.059	3	0.1987	4.6	4.78 (7)	-1.32 ± 0.03	-1.32 ± 0.03	OB91 L
269.9107	44415.074	4	7376.764	4	0.2315	4.4	5.57 (7)	-1.26 ± 0.03	-1.26 ± 0.02	OB91 L
266.6812	44415.074	4	6928.268	5	0.3765	3.6	9.05 (6)	-1.061 ± 0.03	-1.07 ± 0.02	OB91 L

Table 4—Continued

Wavelength ^a (nm)	Upper Level ^a		Lower Level ^a		BF ^b	U _{BF} ^b (%)	A _{ul} ^c (10 ⁶ s ⁻¹)	This experiment ^d log(<i>gf</i>)	Published ^e	
	<i>E</i> (cm ⁻¹)	<i>J</i>	<i>E</i> (cm ⁻¹)	<i>J</i>					log(<i>gf</i>)	Ref.
227.2070	44415.074	4	415.933	3	0.1170	5.1	2.81 (7)	-1.71 ± 0.03	-1.69 ± 0.02	OB91 L
225.0790	44415.074	4	0.000	4	0.0419	6.3	1.01 (8)	-2.16 ± 0.03	-2.08 ± 0.05	OB91 L
273.0982	44760.746	1	8154.713	1	0.1185	6.0	5.56 (8)	-1.73 ± 0.03	-1.68 ± 0.02	OB91 L
271.8436	44760.746	1	7985.784	2	0.7738	1.4	36.33 (5)	-0.92 ± 0.02	-0.90 ± 0.02	OB91 L
228.3304	44760.746	1	978.074	0	0.0510	8.3	2.39 (10)	-2.25 ± 0.04	-2.22 ± 0.02	OB91 L
226.9099	44760.746	1	704.007	2	0.0383	10.5	1.80 (12)	-2.38 ± 0.05		
1033.3185	46720.842	4	37045.932	4	0.0010	12.8	0.09 (14)	-1.91 ± 0.06		
721.9682	46720.842	4	32873.630	4	0.0065	6.9	0.53 (9)	-1.43 ± 0.04		
451.4184	46720.842	4	24574.653	4	0.0049	11.2	0.40 (12)	-1.96 ± 0.05	-1.92 ± 0.18	MA74
435.8501	46720.842	4	23783.617	5	0.0129	5.4	1.06 (7)	-1.57 ± 0.03	-1.68 ± 0.05	OB91 P
399.8052	46720.842	4	21715.731	5	0.0875	4.7	7.17 (7)	-0.81 ± 0.03	-0.91 ± 0.04	OB91 P
383.3308	46720.842	4	20641.109	4	0.0647	5.1	5.30 (7)	-0.98 ± 0.03	-1.032 ± 0.004	BL82b
342.7120	46720.842	4	17550.180	3	0.6593	1.9	54.04 (5)	-0.067 ± 0.02	-0.10 ± 0.04	OB91 P
287.7301	46720.842	4	11976.238	4	0.0544	7.2	4.46 (9)	-1.30 ± 0.04	-1.29 ± 0.04	OB91 P
254.0916	46720.842	4	7376.764	4	0.0067	14.0	0.55 (15)	-2.32 ± 0.06		
251.2275	46720.842	4	6928.268	5	0.0352	7.2	2.89 (9)	-1.61 ± 0.04	-1.73 ± 0.06	OB91 P
215.8920	46720.842	4	415.933	3	0.0128	13.4	1.05 (14)	-2.18 ± 0.06		
213.9698	46720.842	4	0.000	4	0.0369	8.7	3.02 (10)	-1.73 ± 0.04		
553.2747	46889.142	4	28819.952	5	0.0035	14.5	0.31 (15)	-1.89 ± 0.06	-2.10 ± 0.30	MA74
493.4084	46889.142	4	26627.607	4	0.0014	17.9	0.13 (19)	-2.39 ± 0.07		
448.0137	46889.142	4	24574.653	4	0.0048	11.7	0.43 (13)	-1.93 ± 0.05	-1.93 ± 0.09	OB91 P
432.6753	46889.142	4	23783.617	5	0.0068	9.8	0.62 (11)	-1.81 ± 0.05	-1.93 ± 0.09	OB91 P
397.1322	46889.142	4	21715.731	5	0.0583	8.6	5.25 (10)	-0.95 ± 0.04	-0.98 ± 0.04	OB91 P
380.8729	46889.142	4	20641.109	4	0.0387	8.9	3.48 (10)	-1.17 ± 0.04	-1.159 ± 0.004	BL82b
340.7460	46889.142	4	17550.180	3	0.6629	2.8	59.72 (6)	-0.029 ± 0.02	-0.02 ± 0.04	OB91 P
286.3430	46889.142	4	11976.238	4	0.0462	7.3	4.16 (9)	-1.34 ± 0.04	-1.34 ± 0.04	OB91 P
250.1694	46889.142	4	6928.268	5	0.0524	7.4	4.72 (9)	-1.40 ± 0.04	-1.51 ± 0.05	OB91 P
213.2017	46889.142	4	0.000	4	0.0386	9.3	3.48 (11)	-1.67 ± 0.04	-1.33 ± 0.06	

Table 4—Continued

Wavelength ^a (nm)	Upper Level ^a		Lower Level ^a		BF ^b	U _{BF} ^b (%)	A _{ul} ^c (10 ⁶ s ⁻¹)	This experiment ^d log(<i>gf</i>)	Published ^e	
	<i>E</i> (cm ⁻¹)	<i>J</i>	<i>E</i> (cm ⁻¹)	<i>J</i>					log(<i>gf</i>)	Ref.
730.7931	47092.712	3	33412.715	3	0.0228	5.7	1.26 (8)	-1.15 ± 0.03	-1.53 ± 0.06	OB91 P
435.1544	47092.712	3	24118.817	4	0.0210	4.7	1.15 (7)	-1.64 ± 0.03	-1.73 ± 0.04	OB91 P
412.1802	47092.712	3	22838.321	2	0.0539	3.9	2.96 (6)	-1.28 ± 0.03	-1.45 ± 0.04	OB91 P
398.3956	47092.712	3	21999.129	4	0.1291	3.5	7.09 (6)	-0.93 ± 0.03	-1.02 ± 0.04	OB91 P
383.7135	47092.712	3	21038.986	2	0.0177	5.4	0.97 (7)	-1.82 ± 0.03	-1.78 ± 0.09	OB91 P
381.3058	47092.712	3	20874.481	3	0.1163	2.9	6.39 (6)	-1.01 ± 0.02	-1.07 ± 0.04	OB91 P
377.9416	47092.712	3	20641.109	4	0.0112	10.8	0.61 (12)	-2.036 ± 0.05	-1.99 ± 0.05	OB91 P
340.4354	47092.712	3	17726.987	2	0.2180	4.3	11.98 (7)	-0.84 ± 0.03	-0.88 ± 0.04	OB91 P
338.3979	47092.712	3	17550.180	3	0.1494	4.8	8.21 (7)	-1.006 ± 0.03	-1.11 ± 0.04	OB91 P
292.9618	47092.712	3	12968.553	2	0.0135	11.2	0.74 (12)	-2.18 ± 0.05	-2.22 ± 0.05	OB91 P
289.5035	47092.712	3	12560.933	3	0.1089	6.5	5.98 (8)	-1.28 ± 0.03	-1.43 ± 0.04	OB91 P
284.6830	47092.712	3	11976.238	4	0.0164	9.0	0.90 (10)	-2.12 ± 0.04	-2.13 ± 0.04	OB91 P
253.9587	47092.712	3	7728.059	3	0.0072	16.6	0.40 (17)	-2.57 ± 0.07		
251.7123	47092.712	3	7376.764	4	0.0321	7.3	1.77 (9)	-1.93 ± 0.04		
215.5020	47092.712	3	704.007	2	0.0157	25.2	0.86 (26)	-2.38 ± 0.10		
214.1718	47092.712	3	415.933	3	0.0212	15.3	1.16 (16)	-2.25 ± 0.07		
744.3022	47197.010	2	33765.304	2	0.0125	13.0	0.55 (14)	-1.64 ± 0.06		
437.3561	47197.010	2	24338.765	3	0.0230	6.7	1.01 (8)	-1.84 ± 0.04	-1.83 ± 0.09	OB91 P
437.2987	47197.010	2	24335.764	2	0.0064	22.6	0.28 (23)	-2.40 ± 0.09	-2.58 ± 0.18	MA74
412.2516	47197.010	2	22946.814	1	0.0710	5.7	3.10 (8)	-1.40 ± 0.03	-1.39 ± 0.04	OB91 P
410.4154	47197.010	2	22838.321	2	0.0073	8.8	0.32 (10)	-2.40 ± 0.04		
382.1835	47197.010	2	21038.986	2	0.1889	4.7	8.25 (7)	-1.044 ± 0.03	-1.10 ± 0.04	OB91 P
341.5531	47197.010	2	17927.381	1	0.0839	6.6	3.67 (8)	-1.49 ± 0.04	-1.39 ± 0.05	OB91 P
339.2305	47197.010	2	17726.987	2	0.1783	5.8	7.79 (8)	-1.17 ± 0.03	-1.07 ± 0.05	OB91 P
292.0691	47197.010	2	12968.553	2	0.1060	7.2	4.63 (9)	-1.53 ± 0.04	-1.39 ± 0.04	OB91 P
288.6317	47197.010	2	12560.933	3	0.0335	10.8	1.47 (12)	-2.039 ± 0.05	-2.09 ± 0.04	OB91 P
256.0557	47197.010	2	8154.713	1	0.0405	7.7	1.77 (9)	-2.061 ± 0.04	-2.11 ± 0.04	OB91 P
254.9525	47197.010	2	7985.784	2	0.0081	21.3	0.35 (22)	-2.77 ± 0.09	-2.49 ± 0.05	OB91 P
253.2876	47197.010	2	7728.059	3	0.0328	8.0	1.43 (10)	-2.16 ± 0.04	-2.16 ± 0.04	OB91 P
215.0185	47197.010	2	704.007	2	0.0311	18.2	1.36 (19)	-2.33 ± 0.08		

Table 4—Continued

Wavelength ^a (nm)	Upper Level ^a		Lower Level ^a		BF ^b	U _{BF} ^b (%)	A _{ul} ^c (10 ⁶ s ⁻¹)	This experiment ^d log(<i>gf</i>)	Published ^e	
	<i>E</i> (cm ⁻¹)	<i>J</i>	<i>E</i> (cm ⁻¹)	<i>J</i>					log(<i>gf</i>)	Ref.
393.5307	48350.606	1	22946.814	1	0.0102	16.0	0.91 (17)	-2.199 ± 0.07	-1.82 ± 0.18	MA74
328.6016	48350.606	1	17927.381	1	0.0106	20.6	0.94 (21)	-2.34 ± 0.08		
326.4513	48350.606	1	17726.987	2	0.0261	15.2	2.33 (16)	-1.95 ± 0.06	-1.32 ± 0.05	OB91 P
248.7066	48350.606	1	8154.713	1	0.6014	2.6	53.70 (6)	-0.83 ± 0.02	-0.75 ± 0.05	OB91 P
247.6657	48350.606	1	7985.784	2	0.2956	4.9	26.39 (7)	-1.14 ± 0.03	-1.08 ± 0.04	OB91 P
537.9574	48382.603	5	29798.934	4	0.0128	3.9	0.79 (6)	-1.42 ± 0.03	-1.51 ± 0.04	OB91 P
524.2491	48382.603	5	29313.006	6	0.0526	2.7	3.25 (6)	-0.83 ± 0.02	-0.97 ± 0.04	OB91 P
511.0358	48382.603	5	28819.952	5	0.0148	4.0	0.91 (6)	-1.41 ± 0.03	-1.37 ± 0.04	OB91 P
459.5358	48382.603	5	26627.607	4	0.0087	5.0	0.54 (7)	-1.73 ± 0.03	-1.76 ± 0.04	OB91 P
419.9095	48382.603	5	24574.653	4	0.8193	0.6	50.57 (5)	0.17 ± 0.02	0.16 ± 0.04	OB91 P
412.0206	48382.603	5	24118.817	4	0.0345	3.1	2.13 (6)	-1.23 ± 0.03	-1.27 ± 0.04	OB91 P
378.9176	48382.603	5	21999.129	4	0.0317	4.1	1.96 (7)	-1.33 ± 0.03	-1.29 ± 0.04	OB91 P
360.3681	48382.603	5	20641.109	4	0.0060	11.7	0.37 (13)	-2.10 ± 0.05	-2.01 ± 0.08	OB91 P
347.5863	48382.603	5	19621.005	5	0.0115	18.4	0.71 (19)	-1.85 ± 0.08		
470.8969	50586.878	3	29356.742	2	0.0068	28.4	0.37 (29)	-2.07 ± 0.11	-2.03 ± 0.09	OB91 P
454.7847	50586.878	3	28604.611	2	0.1279	2.1	6.91 (6)	-0.82 ± 0.02	-1.01 ± 0.12	OB91 P
417.1900	50586.878	3	26623.733	2	0.0221	6.1	1.20 (8)	-1.66 ± 0.03	-1.70 ± 0.05	OB91 P
410.3611	50586.878	3	26224.967	3	0.0022	18.8	0.12 (20)	-2.67 ± 0.08		
384.3257	50586.878	3	24574.653	4	0.7374	0.8	39.86 (5)	-0.21 ± 0.02	-0.24 ± 0.04	OB91 P
380.8282	50586.878	3	24335.764	2	0.0177	16.3	0.95 (17)	-1.84 ± 0.07	-1.94 ± 0.06	OB91 P
352.7891	50586.878	3	22249.428	3	0.0148	21.3	0.80 (22)	-1.98 ± 0.09		
302.6056	50586.878	3	17550.180	3	0.0161	26.2	0.87 (27)	-2.077 ± 0.10		
697.7429	51373.910	5	37045.932	4	0.0068	10.7	0.47 (12)	-1.42 ± 0.05		
540.3822	51373.910	5	32873.630	4	0.0319	3.1	2.20 (6)	-0.98 ± 0.03	-1.03 ± 0.05	OB91 P
453.1636	51373.910	5	29313.006	6	0.0048	12.1	0.33 (13)	-1.95 ± 0.05		
443.2568	51373.910	5	28819.952	5	0.0117	12.0	0.80 (13)	-1.58 ± 0.05	-1.56 ± 0.18	MA74
395.6455	51373.910	5	26105.906	6	0.2287	2.5	15.77 (6)	-0.39 ± 0.02	-0.34 ± 0.04	OB91 P
373.0386	51373.910	5	24574.653	4	0.1296	4.9	8.94 (7)	-0.69 ± 0.03	-0.65 ± 0.04	OB91 P

Table 4—Continued

Wavelength ^a (nm)	Upper Level ^a		Lower Level ^a		BF ^b	U _{BF} ^b (%)	A _{ul} ^c (10 ⁶ s ⁻¹)	This experiment ^d log(<i>gf</i>)	Published ^e	
	<i>E</i> (cm ⁻¹)	<i>J</i>	<i>E</i> (cm ⁻¹)	<i>J</i>					log(<i>gf</i>)	Ref.
337.0783	51373.910	5	21715.731	5	0.3413	3.9	23.54 (6)	-0.36 ± 0.03	-0.27 ± 0.04	OB91 P
325.2915	51373.910	5	20641.109	4	0.0267	9.8	1.84 (11)	-1.49 ± 0.05	-1.42 ± 0.04	OB91 P
312.5683	51373.910	5	19390.167	6	0.1049	5.7	7.23 (8)	-0.93 ± 0.03	-0.87 ± 0.04	OB91 P
253.7459	51373.910	5	11976.238	4	0.0604	9.6	4.17 (11)	-1.35 ± 0.05	-1.47 ± 0.06	OB91 P
420.3938	53093.528	6	29313.006	6	0.0342	7.2	3.23 (9)	-0.95 ± 0.04	-0.99 ± 0.04	OB91 P
411.8545	53093.528	6	28819.952	5	0.5906	3.2	55.72 (6)	0.27 ± 0.03	0.22 ± 0.04	OB91 P
373.8305	53093.528	6	26351.038	5	0.3624	5.2	34.18 (7)	-0.031 ± 0.03	-0.03 ± 0.04	OB91 P

^aWavelengths, upper and lower energy levels and *J* quantum numbers are taken from Kramida et al. (2011).

^bThe measured branching fraction, BF, is expressed per-unit and its relative uncertainty, $\delta\text{BF}/\text{BF}$, as a percentage.

^cThe measured transition probability, A_{ul}, in 10⁶ s⁻¹. In brackets, its uncertainty expressed in percentage.

^dThe log(*gf*) values measured in this work together with their uncertainty in dex.

^eValues of log(*gf*)s from other authors used for comparison with their uncertainty in dex. The acronyms in the reference column correspond to: BL79 - Blackwell et al. (1979); OB91 - O’Brian et al. (1991); BL82a - Blackwell et al. (1982a); MA74 - May et al. (1974); BL82b - Blackwell et al. (1982b); BA94 - Bard et al. (1994). The letter included after the reference OB91 indicates the method used by the authors, with ‘L’ and ‘P’ standing for ‘lifetime’ and ‘population’ method, respectively.

Table 5. Lines from Table 4 selected for solar synthesis.

λ_{air} (Å)	E_{low} (eV)	VdW ^a parameter	This experiment		Previously published			v_{macro} (km s ⁻¹)	New gf		Previous gf	
			log(<i>gf</i>)	Unc.	log(<i>gf</i>)	Unc. ^b	Ref. ^c		log(ϵ)	RMS ^d	log(ϵ)	RMS ^d
3808.729	2.559	265.262	-1.17	0.04	-1.16	0.00	BL82b	3.2	7.47	0.9	7.46	0.9
4120.206	2.990	338.253	-1.23	0.03	-1.27	0.04	OB91	3.6	7.56	1.9	7.60	2.0
4432.568	3.573	275.254	-1.58	0.05	-1.56	0.18	MA74	3.2	7.39	1.0	7.38	1.0
4447.717	2.223	429.302	-1.36	0.03	-1.34	0.01	BL82a	3.2	7.60	0.6	7.58	0.7
4459.117	2.176	417.302	-1.29	0.03	-1.28	0.01	BL82a	2.5	7.50	0.9	7.49	0.9
4494.563	2.198	416.302	-1.14	0.03	-1.14	0.01	BL82a	3.1	7.46	1.2	7.46	1.2
4514.184	3.047	296.271	-1.96	0.05	-1.92	0.18	MA74	3.2	7.40	1.1	7.36	1.2
4547.847	3.546	313.266	-0.82	0.02	-1.01	0.12	OB91	3.1	7.41	1.5	7.59	1.6
4595.358	3.301	286.270	-1.73	0.03	-1.76	0.04	OB91	3.4	7.60	1.2	7.62	1.2
4630.120	2.279	416.254	-2.58	0.05	-2.59	0.12	OB91	3.0	7.56	1.7	7.56	1.7
4708.969	3.640	-7.800	-2.07	0.11	-2.03	0.09	OB91	4.1	7.92	0.7	7.88	0.7
5379.574	3.695	363.249	-1.42	0.03	-1.51	0.04	OB91	3.2	7.43	0.9	7.53	0.9
5403.822	4.076	-7.810	-0.98	0.03	-1.03	0.05	OB91	3.7	7.62	1.1	7.66	1.1
5532.747	3.573	237.255	-1.89	0.06	-2.10	0.30	MA74	3.4	7.25	0.4	7.45	0.4
7219.682	4.076	-7.740	-1.43	0.04	-1.73		K14	3.1	7.40	0.5	7.70	0.5
7307.931	4.143	-7.810	-1.15	0.03	-1.53	0.06	OB91	3.4	7.33	0.4	7.69	0.5
7443.022	4.186	-7.810	-1.64	0.06	-1.40		K14	3.4	7.47	0.5	7.24	0.5

^aVan der Waals broadening parameter (see text for explanation).

^bUncertainties are only available for experimentally measured log(*gf*) values.

^cReference acronyms are the same as for Table 4. In addition, K14 stands for Kurucz (2014).

^dRMS difference between observed and synthetic flux in percent, for the points included in the fit.